A Rapid, Robust, and Accurate Coupled Boundary-Layer Method for Cart3D

David L. Rodriguez[*], Peter Sturdza[†], Yoshifumi Suzuki[‡], Hervé Martins-rivas[§]
Desktop Aeronautics, Inc., Palo Alto, CA, 94303

Andy Peronto[¶]
Independent Consultant

An interactive boundary-layer method has been implemented within the Cart3D Euler solver. The implementation subscribes to the philosophy of automation and efficiency of the original Euler-based inviscid method. A quasi-simultaneous coupling algorithm has been applied to promote speedy convergence and robustness. A new interface between Cart3D and the boundary layer solver has been invented which further promotes robustness and accuracy. An elliptic solver for propagating the boundary layer solution between the 2-D strips has been developed that exhibits improved accuracy over traditional solvers. Results on airfoils, wings, and full aircraft configurations are shown and compared to Navier-Stokes solutions and experimental data. Conclusions are drawn as to the accuracy and practical application of the method.

Nomenclature

α	angle of attack
C_L	lift coefficient
C_D	drag coefficient
$C_{D,\text{press}}$	drag coefficient due to pressure
$C_{D,\text{visc}}$	drag coefficient due to skin friction
C_f	skin friction coefficient, normalized by the freestream dynamic pressure
C_p	pressure coefficient
δ^*	boundary layer displacement thickness
$\dot{m}$	local surface transpiration flux
M_∞	freestream Mach number
Re_{chord}	freestream Reynolds number based on the airfoil chord
Re_{MAC}	freestream Reynolds number based on a mean aerodynamic chord
ρ_w	flow density at the wall
S	distance along a running length of boundary layer
u	velocity magnitude
u_w	flow velocity at the wall
x/c	fractional location along the chord of a wing

[*] Vice President of Design Technology, Senior AIAA Member

[†] Vice President of Research & Development, AIAA Member

[‡] Engineer/Scientist

[§] Engineer/Scientist

[¶] Engineer/Scientist

I. Background

Cartesian Euler methods have advanced tremendously over the past decade[1-3] and provide significant advantages over body-fitted structured and even unstructured mesh solvers. The ability to automatically generate quality meshes on arbitrarily complex geometries is perhaps the most remarkable advantage to the aircraft designer. Eliminating the often tedious grid-generation process from the workflow dramatically increases efficiency and therefore productivity. This feature also allows for the successful application of Cartesian Euler methods in a multidisciplinary design optimization environment[4-6]. Figure 1 illustrates a typical Cartesian mesh used on the supersonic business jet discussed in reference [6]. Cartesian Euler methods have even been applied in the design of natural laminar flow wings.[7] However, in all of these listed examples, the designs were optimized for supersonic flight where the Reynolds numbers are very high and therefore the boundary layers are extremely thin. Consequently, the viscous effects on the pressure distributions can be and are in fact neglected.
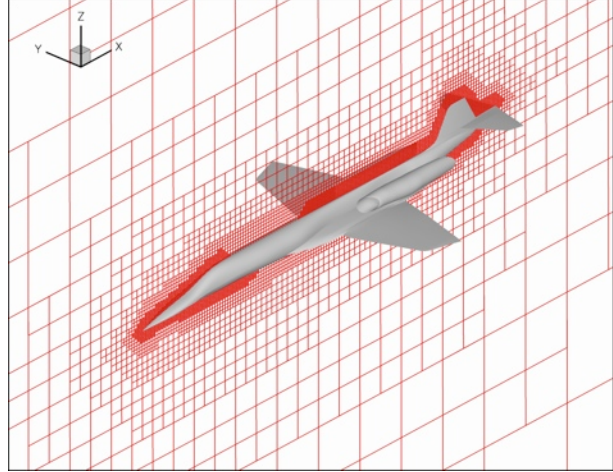

Figure 1. Example Cartesian mesh on a full supersonic business jet configuration.

But this simplification is certainly not justified for subsonic flow and is not even reasonable for transonic flow where Reynolds number effects can be quite significant. Cartesian methods have not yet advanced to the point where accurate viscous solvers can be easily and productively applied because of the unwieldy size of the meshes that are required. However, in past decades when computer hardware was still severely limiting for advanced viscous solvers, Euler and full potential methods were often coupled with interactive boundary layer solvers to produce viscous simulations at a fraction of the cost of Navier-Stokes solutions[8-11]. A similar methodology has been successfully applied to the Cartesian Euler solver, Cart3D[1-2], which produces a relatively accurate viscous simulation method without sacrificing any of the tremendous advantages of original methodology.

An earlier implementation of an interactive-boundary-layer (IBL) method within Cart3D was already completed by Aftosmis et. al.[12] before the work presented in this paper. While the method produced some results that matched Navier-Stokes solutions relatively well, in practice the solver was found to lack robustness and repeatability. Obtaining accurate solutions also often required a great deal of "tuning" of the necessary data-smoothing parameters. These deficiencies forced the implementation to remain a research code and never enter the industry as a productive enhancement to the already widely used Cart3D Euler solver.

In 2007, Desktop Aeronautics initiated the task of improving the IBL method implemented by NASA Ames Research Center. A thorough investigation of past IBL implementations was completed and the more promising methodologies were tested in Cart3D. The final result was a much more robust and accurate Cart3D-IBL solver that did not suffer most of the deficiencies of the original implementation. The boundary-layer solvers themselves are more accurate and some even provide a fast transition prediction capability[13]. This paper will briefly discuss the algorithms and methodologies tested and finally implemented in Cart3D-IBL, though many more details are available in reference [14]. A number of results from this enhanced solver are also presented in later sections.

II. Methodology

The following sub-sections discuss the theory and implementation of the IBL solver in Cart3D. The underlying theory is first discussed along with Cart3D-specific issues. The main boundary layer solver is then presented, followed by details on the coupling algorithm implemented. Finally, details on the interface between Cart3D and the IBL solver are discussed.

A. Basic Interactive Boundary Layer Theory

The underlying premise behind Cart3D-IBL is the same as any other IBL algorithm: the inviscid solver is used to compute the outer flow while the viscous solver solves only the flow right at the surface of the geometry being analyzed. More specifically, it is based on the theory that solving the inviscid flow around a geometry that is displaced by the boundary layer displacement thickness produces the same pressure field as solving the full viscous flow on the original surface geometry. Lock[15] and Lighthill[16] provide much more detail on this theory. Of course,

determining and then solving the flow around the displaced surface geometry is problematic in practice. Fortunately, Lighthill's relation allows the IBL solver to still use the actual surface geometry but then simply alter the boundary condition to mimic the effects of the boundary layer:

$$\dot{m} = \frac{d}{dS}\left(\rho_w u_w \delta^*\right) \qquad (1)$$

Equation (1) computes the local mass flow rate through the surface (or transpiration flux) that correspondingly models the boundary layer displacement thickness in an inviscid flow. The transpiration boundary condition has been successfully used by many IBL solvers [8-11]. Cart3D-IBL not only utilizes Lighthill's relation as a transpiration boundary condition, but also includes a streamline curvature correction discussed by Lock. This curvature correction was found to be critical for accuracy of the solution overall.

On the other hand, many IBL solvers include a wake model to account for the thinning of the boundary layer beyond the trailing edge of an
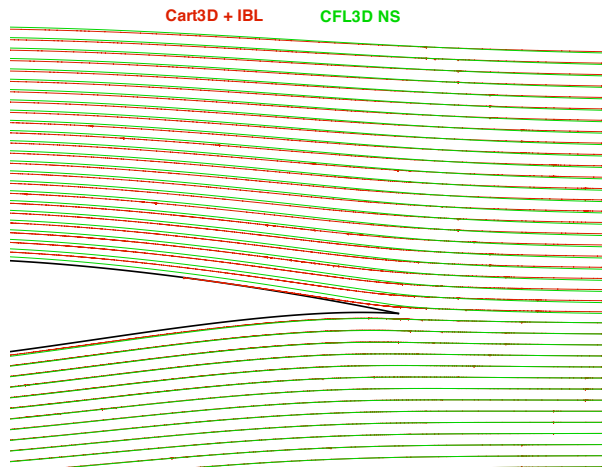

Figure 2. Streamlines at the trailing edge of an airfoil computed by Euler-IBL with no wake model and Navier-Stokes. The red streamlines are from Cart3D-IBL and green from CFL3D (Navier-Stokes).

aerodynamic body such as a wing. Unfortunately, because the discretized Euler equations do not require a wake to maintain the Kutta condition as, for instance, a panel or full-potential code would, there is no geometry behind the trailing edge into which to ingest flow and model the thinning of the wake shear layer. This means the streamlines beyond the trailing edge of a wing turn more rapidly as they converge from the upper and lower surfaces than they would in truly viscous flow. Figure 2 illustrates this phenomenon. This premature turning of the streamlines effectively increases the pressure near the trailing edge, meaning Cart3D-IBL solutions will always recover to slightly higher pressures at the trailing edges of airfoils and wings. This increased pressure at the trailing edge leads to *decreased* pressure drag on the wing or airfoil overall. To solve this problem, a wake model of some kind would need to be introduced into the solver to properly model the thinning of the boundary layer as it leaves a trailing edge. Because Cart3D can handle arbitrarily complex geometry, automatically generating wake panels behind trailing edges is not a trivial task. Further research continues into ways to include a wake model, but for the moment, Cart3D-IBL will always tend to over-predict trailing edge pressures and consequently under-predict pressure drag.

B. Boundary Layer Solver

The main workhorse of the IBL method is the 2-D strip boundary-layer solver. For this implementation, an integral boundary-layer solver based on the work by Drela[17] was selected. An integral method was chosen because previous experience indicates that this type of solver is more robust than those that solve the entire boundary layer profile in a local mesh, especially in small regions of separation. This particular integral solver was chosen because of its well-validated accuracy in the XFOIL[18] code and because it solves the laminar and turbulent parts of the boundary layer simultaneously. Note the more classic solvers, such as the methods of Thwaites and Head only solve either the laminar or turbulent parts but not both. Also, Drela's solver is compressible whereas Thwaites' and Head's are strictly incompressible. Probably the most widely used integral boundary-layer solver, Green's[19] lag-entrainment method, is compressible but only solves turbulent boundary layers. Finally, having separate turbulent and laminar solvers with different numbers of variables and equations poses both numerical and practical programming difficulties when trying to couple those with an inviscid solver, especially when using the full- or quasi-simultaneous approaches. This is the primary reason to use the Drela solver, which was essentially Drela's solution to combining a laminar boundary layer solver with something similar to the lag-entrainment method.

Some results obtained by the implemented boundary-layer code are compared to that of XFOIL for validation purposes. Figure 3 shows the momentum thickness and skin friction coefficient distributions on a NACA 0012 airfoil. The freestream Mach and chord Reynolds numbers are 0.1 and 100,000 respectively. In this example, the flow remains laminar on the entire surface and agrees well with the XFOIL result. A second example, presented in Figure 4, shows the same flow forced to transition at 20% chord with the same freestream conditions as the first example except the Reynolds number is 1,000,000. Both examples exhibit excellent agreement with XFOIL results attesting to the accuracy of the Cart3D-IBL boundary layer solver.
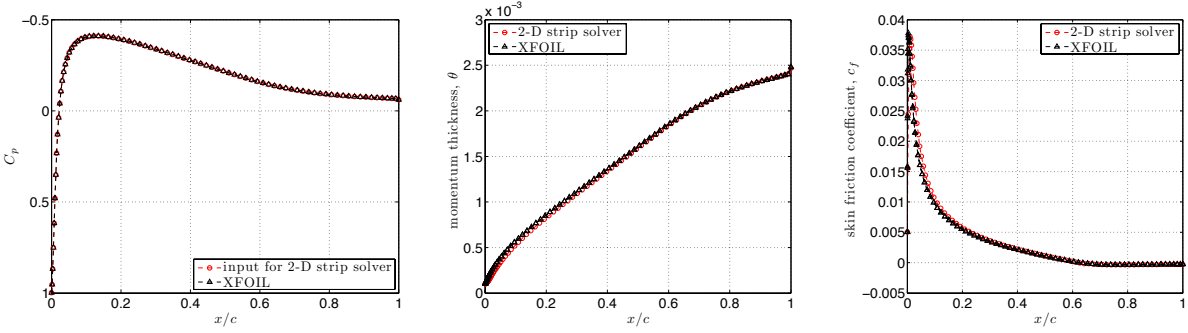
Figure 3. Comparison of fully laminar solutions from XFOIL (red) and the Cart3D-IBL 2-D solver (blue) on a NACA 0012 airfoil at $M_\infty = 0.1$, $\alpha = 0$, $Re_{chord} = 100,000$.
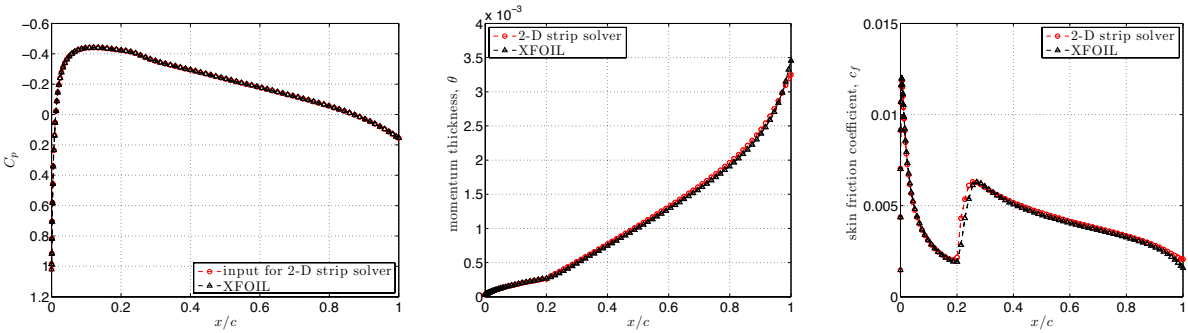

Figure 4. Comparison of partially turbulent solutions from XFOIL (red) and the Cart3D-IBL 2-D strip solver (blue) on a NACA 0012 airfoil at $M_\infty = 0.1$, $\alpha = 0$, $Re_{chord} = 1,000,000$. Transition is set at 20% chord.

C. Interactive Coupling Algorithms

In the process of improving the robustness and speed of Cart3D-IBL, several interactive-boundary-layer coupling techniques were evaluated. The simplest and most intuitive interaction scheme is the so-called direct method. It is given that name because both the inviscid and the boundary-layer solvers are evaluated in direct, rather than inverse modes. More specifically, the inviscid solver provides a pressure or velocity distribution to the boundary layer solver which computes a boundary layer thickness distribution. However, the direct method has some serious limitations. In flows with strong interaction between the viscous and inviscid portions (such as those shown in Figure 5 from reference [20]), considerable under-relaxation is required to stabilize and converge the method. Experience with the scheme has also shown that the amount of under-relaxation usually must increase as the inviscid, computational mesh size grows rendering the method impractical for subsonic and transonic cases. On the other hand, for purely supersonic flows the direct method works reasonably well. More details on the direct method are presented in reference [14].

Another commonly implemented viscous-inviscid coupling technique is the semi-inverse method of Carter[21]. In this algorithm, the inverse boundary-layer solver is provided an estimation of the displacement thickness distribution from which it computes the edge velocity/pressure distribution. An interaction formula is then used to drive both the inviscid and viscous solvers to agree on the edge velocity distribution. This method was used extensively by Cebeci and his colleagues at the former Douglas Aircraft Company with inviscid panel methods and even Euler codes[22]. The rationale for the method is that since the direct-mode boundary-layer equations become singular at separation points but the inverse-mode equations do not, then using an inverse boundary-layer code in the viscous-inviscid system would circumvent the problems with the direct method. When implemented in Cart3D, the semi-inverse method seemed to work and certainly provided more stability, but its rate of convergence was
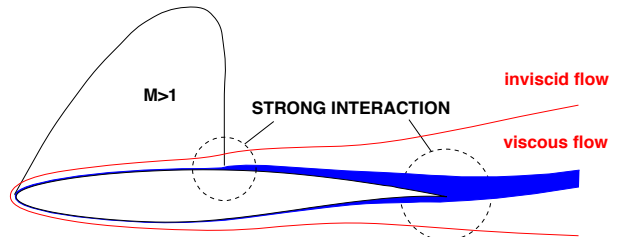

Figure 5. Areas of closely-coupled viscous-inviscid interaction (image courtesy of Prof. Arthur Veldman).

not particularly impressive. Also, it was discovered that the still-necessary level of under-relaxation continued to depend on the size of the inviscid computational mesh. Due to the nature of Cartesian-mesh flow solvers, relatively fine meshes are required at leading and trailing edges of wings and therefore the semi-inverse method was not deemed ideal for Cart3D-IBL. Again, more details on the semi-inverse method are presented in reference [14].

Figure 6. Quasi-simultaneous method.

Of course, the ideal coupling scheme, called the fully simultaneous method, involves adding the boundary-layer equations to the inviscid flow equations and solving them all together as one large set of equations. This method has been used with great success by Drela[18] in two dimensions. But the real difficulty for a Cart3D-IBL implementation is that the existing explicit flow solver is not compatible with the fully simultaneous method and would essentially need to be completely rewritten.

The next-best technique is due to Veldman[20,23] and is known as the quasi-simultaneous method. It involves a fully simultaneous solution of the boundary-layer equations with an approximation of the inviscid flow followed by what amounts to a direct-method style coupling between that system and the true inviscid solver (as depicted in Figure 6). Veldman generally uses incompressible thin airfoil theory as the approximation to the inviscid flow and calls it the interaction law. For the Cart3D-IBL solver, this method was taken one step further and uses a 2-D panel code as the approximate flow solver which provided added stability to the method overall. Reference [14] provide a great many more details on the implementation in the Cart3D-IBL solver.
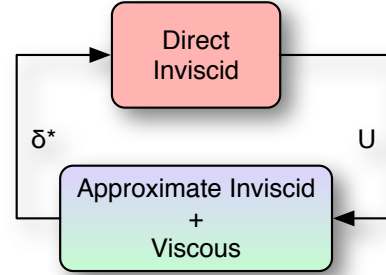
D. Interface Between Cart3D and the Boundary Layer Solver

The embedded boundary conditions used in Cart3D present an interesting challenge in interfacing the boundary-layer and Euler solvers. Traditionally with structured inviscid codes that couple with an IBL solver, the boundary layer mesh and the inviscid mesh line up exactly in the streamwise direction. This is illustrated in Figure 7. Data from the inviscid solver is available at the wall in the exact location where a quality boundary layer mesh can be generated. Of course, with an integral method, the mesh can simply be a grid line from the inviscid mesh surface. However, Cart3D uses an unstructured, triangulated surface to drive the embedded boundary condition in the volume mesh cells intersected by the surface (cut-cells). The original Cart3D-IBL implementation[12] used flow data from the surface triangulation to drive the boundary layer solver. Since the triangulation topology does not necessarily lend itself to smooth slices of geometry on which to solve the boundary layer, the data is always interpolated to some slice of the triangulation. Of course, the data on the triangulation is already interpolated from the volume mesh solutions. Normally, there is not a one-to-one connection between a volume cell and a surface mesh cell; in fact, usually there are many more surface mesh cells in the streamwise direction to ensure accuracy of the Euler solver. To compound matters, the original boundary layer solver required an equispaced mesh in the streamwise direction, forcing yet another interpolation and resampling of data in the streamwise direction. These multiple layers of inter-
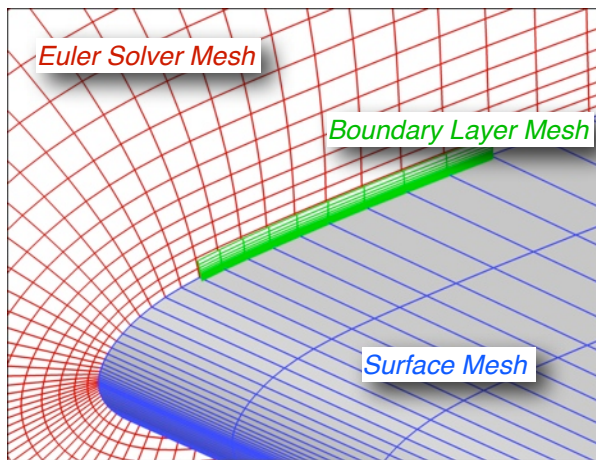

Figure 7. Topology on a typical IBL implementation on a structured mesh. All meshes match cell by cell making data interface between solvers straightforward.
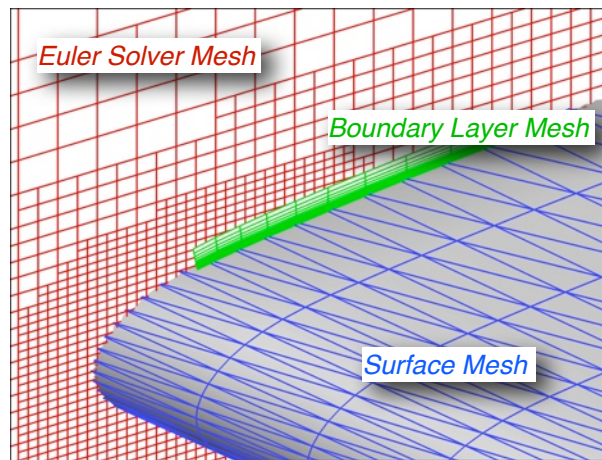

Figure 8. Topology of IBL implementation on a Cart3D mesh. The triangulation on the surface is shown coarse here but is typically finer than the Cartesian mesh.

polation from the cut-cells to the triangulation and from the triangulation to the boundary layer mesh provide multiple sources of error, especially since there are rarely one-to-one interpolations in any layer. The accumulated error would result in very rough data which would have to be numerically smoothed to allow the boundary layer solver to function properly, introducing yet another source of error. In the end, the interface was error-prone and not robust.

To diminish these errors and consequently improve robustness, the interface was completely reinvented. The original interface was crippled by the fact that the boundary layer solver required equally spaced solution points in the streamwise direction. The boundary layer developed in this work has no such restriction. This allows for drastic simplification of the interface. Instead of the triangulation dictating the boundary layer mesh, the volume mesh

Figure 9. Volume grid and corresponding boundary-layer points on a typical wing section.

itself determines the mesh. The volume mesh is sliced and each cut-cell that intersects the boundary provides a boundary layer mesh point. An example is shown in Figure 9. The red dots and blue squares represent a boundary layer mesh for the integral solver. Data is transferred from the cut-cell to the boundary layer solver with minimal 1st-order accurate interpolation (within the cell only, from the cell center to surface), minimizing error. Unfortunately, the nature of the inviscid solution can will still produce slightly oscillatory data which occasionally will require a tiny amount of numerical smoothing. However, most often the flow data can be used in raw form with no ill effects. This new interface along with the quasi-simultaneous coupling scheme discussed above drastically improved robustness and accuracy of the Cart3D-IBL solver.
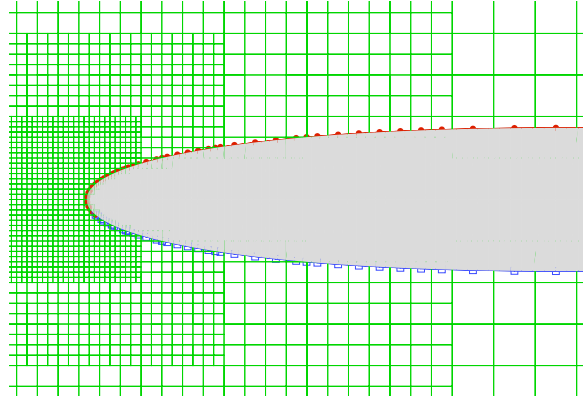
E. Elliptic Solver

The boundary-layer solver only solves the boundary layer on 2-D cuts or strips of the full geometry. In order to model the boundary layer on the entire 3-D surface of a configuration, the set of 2-D local solutions must be converted into a 3-D solution over the entire surface of the configuration being analyzed. The actual task that must be completed is interpolation and even extrapolation the transpiration flux over the entire surface given the transpiration flux on the 2-D boundary layer strips. The most common technique for doing so is to solve the diffusion equation over the entire surface with the boundary-layer solution strips acting as fixed boundary conditions. This is what was done by both Potsdam[11] and Aftosmis[12]. This algorithm that solves the diffusion equation is commonly referred to as the "elliptic solver" since it is solving the strictly-elliptic diffusion equation. Currently the elliptic solver works on the triangulated surface mesh that acts as the surface representation in the Cart3D flow solver. The solutions from the boundary layer strip solutions are first "seeded" onto the appropriate cells in the triangulation and the elliptic solver then propagates this solution to all other cells on the surface, attempting to mimic a full 3-D boundary layer. An example of this seeding is shown in Figure 10, where the red cells are where the transpiration flux is computed by the boundary layer solver and the blue region must be computed by the elliptic solver.
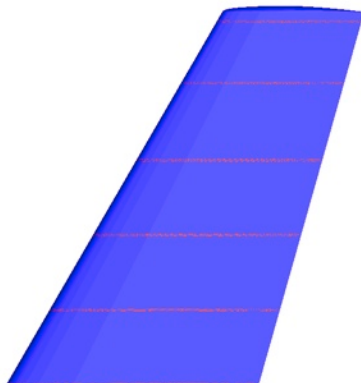

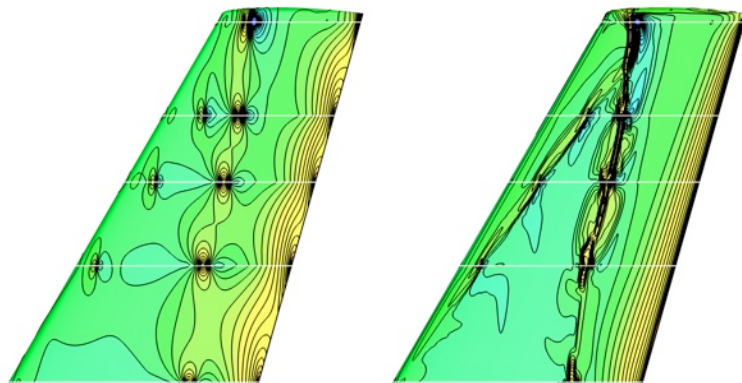**Figure 10. Example of seeded initial condition for elliptic solver on the Onera M6 wing.**

Figure 11. Transpiration flux contours computed by the original (left) and anisotropic (right) on the Onera M6 wing. The white lines indicate where the boundary layer solution strips are located.

Since the initial implementation, two major improvements have been made to the elliptic solver used by Aftosmis[12]. The first improvement was to make the solver grid-independent. The original elliptic solver which used a point-implicit, successive over-relaxation scheme[24], but its accuracy was severely tied to the mesh quality. The new method is based on the SUSHI solver developed by Eymard[25]. More details are discussed in reference [26]. The second improvement was more fundamental and attempted to improve accuracy. Instead of using an isotropic solver, the anisotropic diffusion equation is solved on the triangulation. Since boundary layer thickness is directly related to the local pressure distribution, the isobars are used as directions of maximum diffusion in the anisotropic solver. This allows sharp features such as the large boundary layer growth at the foot of a shock to be maintained between boundary layer strips. This new process allows for fewer boundary layer strips and a better approximation of the full 3-D boundary layer. Figure 11 shows some results from both the original solver and the new anisotropic solver. Notice the transpiration flux contours follow the shock more closely in the anisotropic case and do not have islands of high transpiration as compared to the results for the original solver. More examples are given in reference [26].

III. Applications

Several validation cases were compiled for the Cart3D-IBL solver. In all cases, the Cart3D-IBL results are compared to Reynolds-averaged Navier-Stokes solutions (either CFL3D[27] or OVERFLOW[28]) and in some cases with experimental data. Included in these test cases are several airfoils and a few full 3-D configurations.

Joukowski Airfoil

This airfoil was selected as a test case because it has a cusped trailing edge. The hope was to minimize the effect of the wake on the solution since the upper and lower surfaces of the airfoil are parallel at the trailing edge. However, the curvature of the airfoil surface is still finite as is the curvature of the boundary layer so the lack of wake model is not completely eliminated.

The computed chordwise pressure distributions are shown in Figure 12. The agreement is excellent in this case, with the Cart3D-IBL solution matching the CFL3D Baldwin-Lomax[29] solution perfectly except right at the trailing edge. The turbulence model in Cart3D-IBL is algebraic like the Baldwin-Lomax model so those two solutions should indeed match well. The other solutions use the Spalart-Allmaras[30] one-equation model and Menter's[31] SST two-equation model. The trailing edge pressures are slightly off, presumably because of the lack of a wake model. In fact, as will be obvious in all cases presented here, the trailing edge pressures will always be over-predicted due to the missing wake model.

The computed lift and drag on this airfoil are given in Table 1. The lift forces computed by Cart3D-IBL and CFL3D with the Baldwin-Lomax model are effectively identical. This is expected because of the excellent agreement in the pressure distributions in Figure 12. On the other hand, the total drag by Cart3D-IBL is significantly different than the Navier-Stokes computations. The lower pressure drag is explained primarily by the higher trailing edge pressures in the Cart3D-IBL solution. On the other hand, the viscous component of the drag matches extremely well. Since this is a 2-D subsonic case, the pressure drag is solely due to viscous effects. The missing wake model therefore has a significant effect on the pressure drag. As will be revealed below, for cases where wave and/or induced drag are present, the error due to the missing wake model are diminished compared to the overall drag levels.
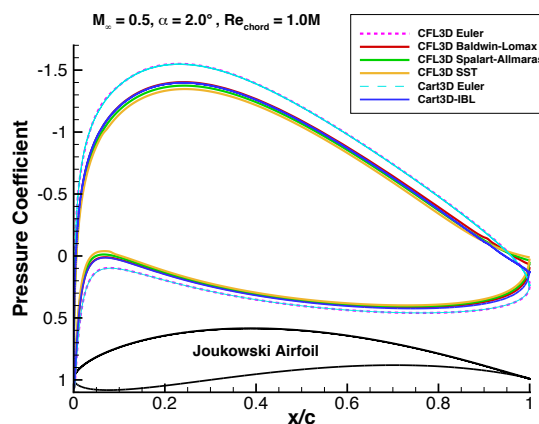
Figure 12. Chordwise pressure distributions computed by Cart3D-IBL and CFL3D (with several turbulence models) on a Joukowski airfoil.

Solver	C_L	C_D	$C_{D,press}$	$C_{D,visc}$
CFL3D (BL)	1.159	0.01608	0.00750	0.00858
CFL3D (SA)	1.123	0.01574	0.00749	0.00825
CFL3D (SST)	1.088	0.01602	0.00795	0.00806
Cart3D-IBL	1.154	0.01375	0.00509	0.00866

Table 1. Computed forces on the Joukowski airfoil analyzed at $M_\infty = 0.5$, $\alpha = 2.0°$, and $Re_{chord} = 1.0$ million. The three CFL3D entries are with three different turbulence models.
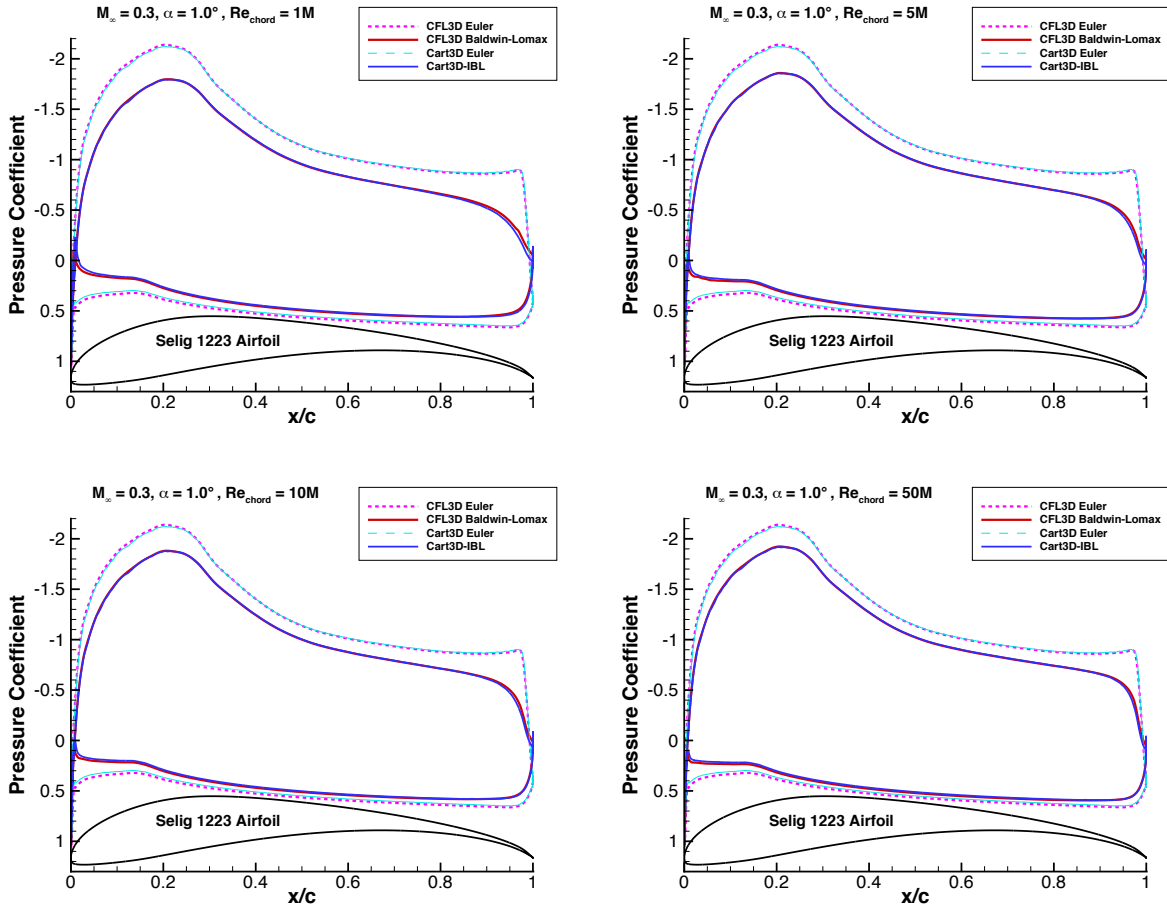
Figure 13. Chordwise pressure distributions from Cart3D and CFL3D solutions for a sweep of Reynolds numbers on the Selig 1223 airfoil.

Selig 1223 Airfoil

This strange airfoil was selected as a test case because of the huge difference between viscid and inviscid solutions, even at low subsonic speeds. Solutions from a range of Reynolds numbers are presented in Figure 13 in the form of chordwise pressure distributions. The comparison between Cart3D-IBL and CFL3D (with the Baldwin-Lomax turbulence model) are near perfect except right at the trailing edge again because of the lack of a wake model.

The computed forces are also given in Table 2.

Solver	C_L	C_D	$C_{D,press}$	$C_{D,visc}$
CFL3D	1.494	0.01327	0.00604	0.00723
Cart3D-IBL	1.425	0.01201	0.00525	0.00676

Table 2. Computed forces on the Selig 1223 airfoil analyzed at $M_\infty = 0.3$, $\alpha = 1.0°$, and $Re_{chord} = 5.0$ million.

Once again, the agreement is quite good in terms of lift, while the pressure drag is under-predicted. In this case, however, the viscous drag is also somewhat under-predicted. Note that the CFL3D solution is slightly unsteady because of a small separation bubble very near the trailing edge on the upper surface. It is certainly possible that this is affecting the viscous drag computation in CFL3D. Once again, a wake model should help improve this drag prediction.

RAE 2822 Airfoil

This airfoil was the first true transonic test of the Cart3D-IBL solver. Some results are show in Figure 14 as compared to Navier-Stokes solutions and experimental data[32]. The shock location for this case falls within the range of the Navier-Stokes solutions with different turbulence models. Note that not only has the IBL solution moved the

Solver	C_L	C_D	$C_{D,\text{press}}$	$C_{D,\text{visc}}$
CFL3D (BL)	0.738	0.01322	0.00685	0.00637
CFL3D (SA)	0.699	0.01308	0.00639	0.00669
CFL3D (SST)	0.693	0.01219	0.00601	0.00618
Cart3D-IBL	0.745	0.01315	0.00705	0.00610

Table 3. Computed forces on the RAE 2822 airfoil analyzed at $M_\infty = 0.729$, $Re_{\text{chord}} = 6.5$ million, and $\alpha = 2.31°$. The three CFL3D entries are with three different turbulence models.
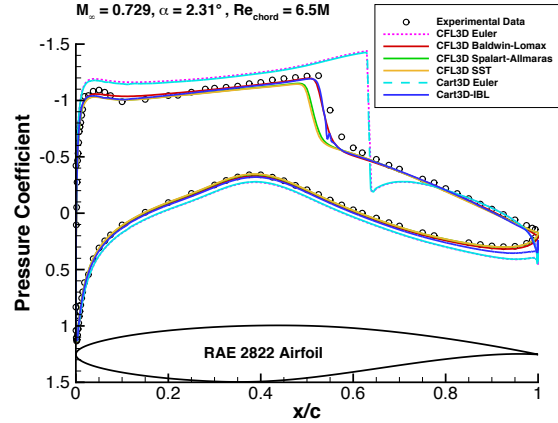

Figure 14. Chordwise pressure distributions from Cart3D and CFL3D solutions (with several turbulence models) on the RAE 2822 airfoil along with experimental data.
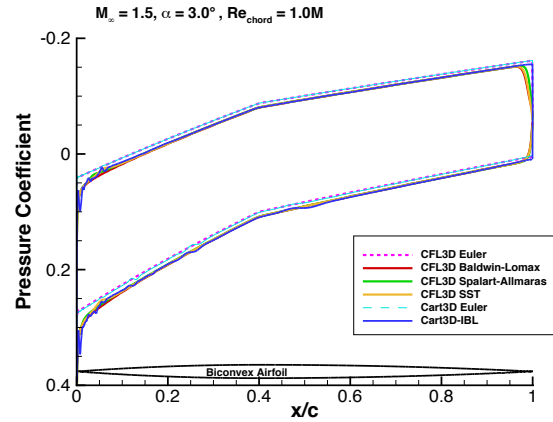

Figure 15. Chordwise pressure distributions from Cart3D and CFL3D solutions (with several turbulence models) on a 3% thick biconvex airfoil.

Solver	C_L	C_D	$C_{D,\text{press}}$	$C_{D,\text{visc}}$
CFL3D (BL)	0.188	0.02225	0.01472	0.00752
CFL3D (SA)	0.189	0.02195	0.01475	0.00720
CFL3D (SST)	0.188	0.02184	0.01471	0.00713
Cart3D-IBL	0.190	0.02339	0.01485	0.00854

Table 4. Computed forces on the 3% biconvex airfoil analyzed at $M_\infty = 1.5$, $\alpha = 3.0°$, and $Re_{\text{chord}} = 1.0$ million. The three CFL3D entries are with three different turbulence models.

shock to the correct location, but it has also eliminated the "Euler bounce", which is the overshoot of pressure followed by a re-acceleration right after a shock in inviscid flow. Also, the IBL solution is slightly ragged right after the shock which is not uncommon with these transonic solutions. Occasionally, for improved stability in transonic cases, a very tiny amount of numerical smoothing must be applied to the data extracted from the Euler solution, which unfortunately introduces very small local errors. This and the fact that the pressure gradients are very high in this region can make it difficult to completely suppress the Euler bounce. Also, the inclusion of a wake model is expected to improve the pressures at the trailing edge, lining it up better with the Navier-Stokes solutions. Note that the wind tunnel geometry used to obtain this experimental data was found to be slightly different than the true RAE 2822 geometry, especially near the leading edge as discussed in reference [32]. This explains the lack of a pressure hump near the leading edge in the CFD solutions. Of course, the goal of Cart3D-IBL is to approach the accuracy of Navier-Stokes solutions which these results indicate has occurred in our implementation.

The computed forces on this case are given in Table 3. In this case, the lift prediction is slightly higher than the Navier-Stokes predictions. The pressure drag, which in this case is mostly wave drag, is somewhat over-predicted while the viscous drag is somewhat higher than the Navier-Stokes calculations. At this point, the reason for this is unclear and further investigation and validation is required.

Biconvex Airfoil

The final 2-D test presented here for the IBL method is a fully supersonic case. A 3% thick biconvex airfoil provides as good of a test as any, especially since this is the only airfoil tested here with a sharp leading edge. This biconvex airfoil has its maximum thickness at 40% chord. The results from Cart3D-IBL and CFL3D are shown in Figure 15. The results are near perfect as

American Institute of Aeronautics and Astronautics

expected since the wake has no effect on the airfoil since all the flow is supersonic. Note, however, that the CFL3D solution smears out the trailing edge shock while Cart3D-IBL maintains a very sharp shock. It is unclear if a wake model would improve this agreement or whether it would even be an improvement.

The computed forces on this biconvex airfoil are given in Table 4. The lift computation agreement is excellent which is not unexpected since the boundary layer has little effect on the lift for this case. In other words, the Euler solution gets about the same lift anyway. However, the drag is slightly over-predicted. Here the pressure drag is predicted well but the viscous drag is a bit high. It is unclear why at this point. Perhaps the turbulence model in the boundary-layer code is not well tuned for supersonic flow. Perhaps the slight difference in the pressures at the trailing edge account for some of this discrepancy. Further investigation will be required to determine the cause of this seemingly over-prediction of viscous drag.

Onera M6 Wing

Cart3D-IBL was also tested in 3-D on the Onera M6 wing. This geometry is often used in validation of CFD codes because of the complex double-shock structure that develops at transonic freestream speeds. Wind tunnel data[33] in the form of pressures are also available for this wing offering an excellent validation case. The Cart3D-IBL solution was generated on the Onera M6 wing using 16 planar cuts parallel to the root for boundary-layer solution strips. The locations of these strips are shown in Figure 16, along with the locations of the available experimentally measured pressures. Note that seven of the IBL strips are placed exactly where the wind tunnel model pressure ports are located.

Figure 17 shows the results from the Cart3D-IBL code on this wing along with the experimental data. For comparison, CFL3D Navier-Stokes solutions are also shown. The agreement between Cart3D-IBL and the experimental data is quite good, especially as compared to the well-validated CFL3D code. Note that the Euler bounce is reduced in the IBL solutions. The Cart3D-IBL solutions at 65% and 80% span are even better than the CFL3D Navier-Stokes solutions. The CFL3D solutions are similar to those documented in the user's manual so it is well known to not perform terribly well on this wing at these span locations. Some streamwise grid refinement studies with CFL3D were performed with no improved results, but it is possible the CFL3D mesh is still too coarse in the spanwise direction. The Cart3D mesh is naturally very refined in the spanwise direction since it must be in the streamwise direction.

A comparison of the forces computed by Cart3D-IBL and the CFL3D solvers is shown in Table 5. The lift calculations agree quite well as expected since the pressures are so similar. Both the pressure and viscous drag predictions are near the high range of Navier-Stokes solutions and are particularly close to the Spalart-Allmaras solution, though this may just be good fortune. Referring back to Figure 17, note that the experimental data does not match terribly well with CFL3D outboard, so perhaps the Cart3D-IBL solution is actually more accurate.

Figure 18 shows the difference in surface pressure contours between the Euler and IBL Cart3D solutions. Note that both shocks are slightly weaker, less crisp, and further forward. The region where the two shocks converge certainly has a softer shock in the IBL solution. This is evidence the Euler undershoot has been diminished as is expected in a viscous solution. Figure 19 shows a comparison of the surface skin friction contours as computed by both CFL3D and Cart3D-IBL. The two plots are very similar except the CFL3D solution has lower skin friction right after the shocks. These levels are very low and the region small, however, so the overall integration of skin friction is not significantly affected.
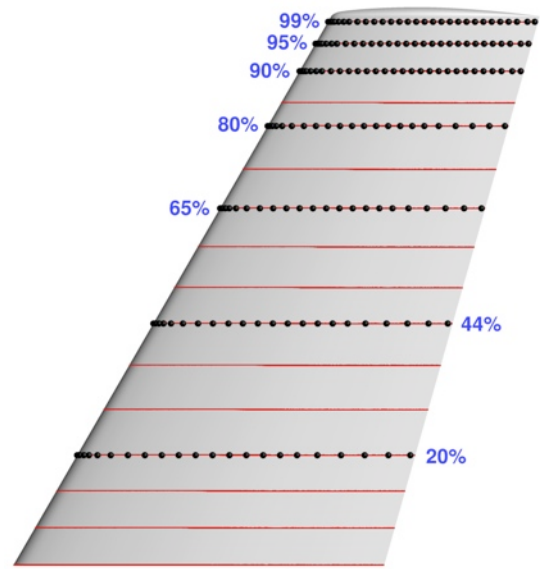

Figure 16. Location of boundary layer strips on the Onera M6 wing for the Cart3D-IBL solution. The black dots are the pressure ports on the wind tunnel model.

Solver	C_L	C_D	$C_{D,\text{press}}$	$C_{D,\text{visc}}$
CFL3D (BL)	0.276	0.01789	0.01245	0.00544
CFL3D (SA)	0.275	0.01914	0.01348	0.00567
CFL3D (SST)	0.267	0.01702	0.01166	0.00536
Cart3D-IBL	0.273	0.01915	0.01350	0.00565

Table 5. Computed forces on the Onera M6 wing analyzed at $M_\infty = 0.8395$, $\alpha = 3.06°$, and $Re_{\text{MAC}} = 11.72$ million. The three CFL3D solutions are with three different turbulence
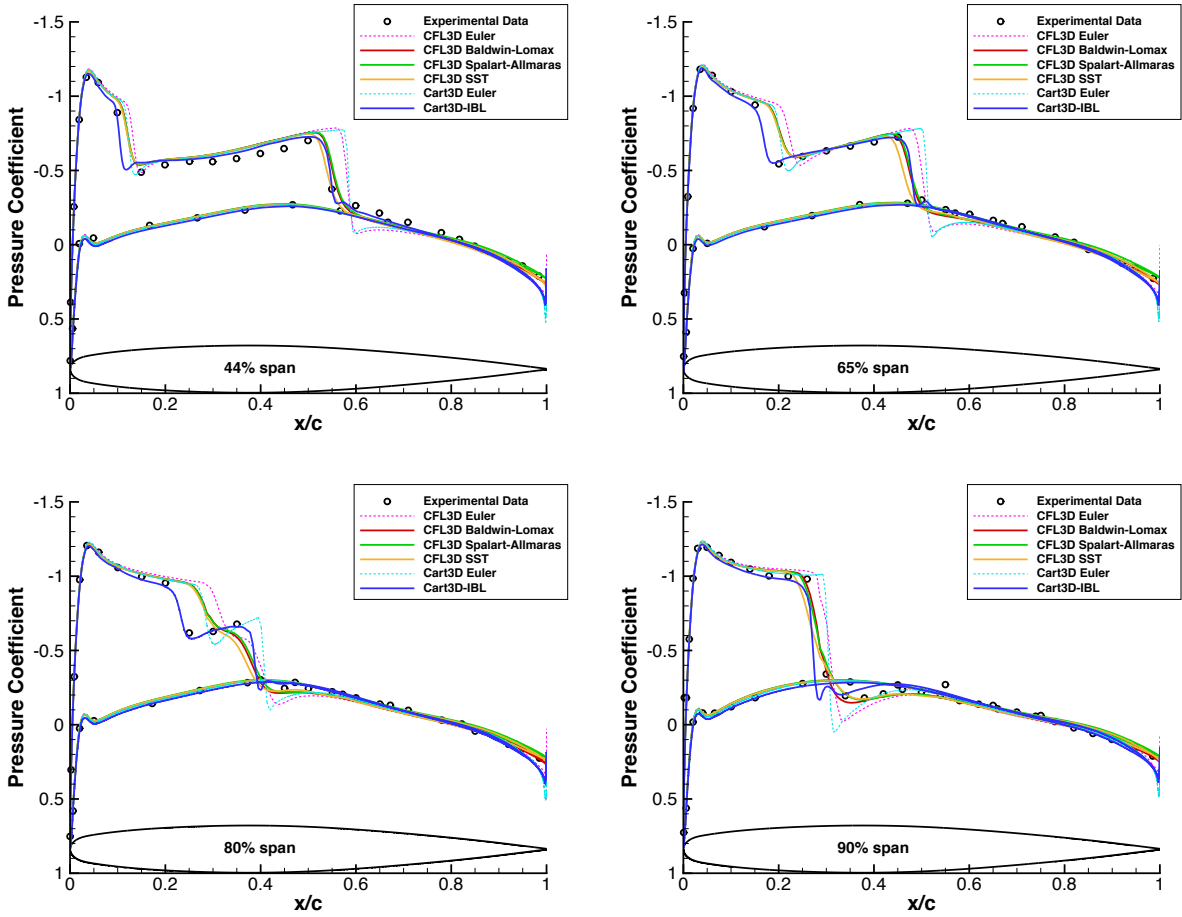
Figure 17. Chordwise pressure distributions at several spanwise stations on the Onera M6 wing at $M_\infty = 0.8395$, $Re_{MAC} = 11.72$ million), and at $\alpha = 3.06°$. Experimental data, CFL3D Navier-Stokes solutions, and Cart3D solutions are shown, including Euler solutions for comparison.
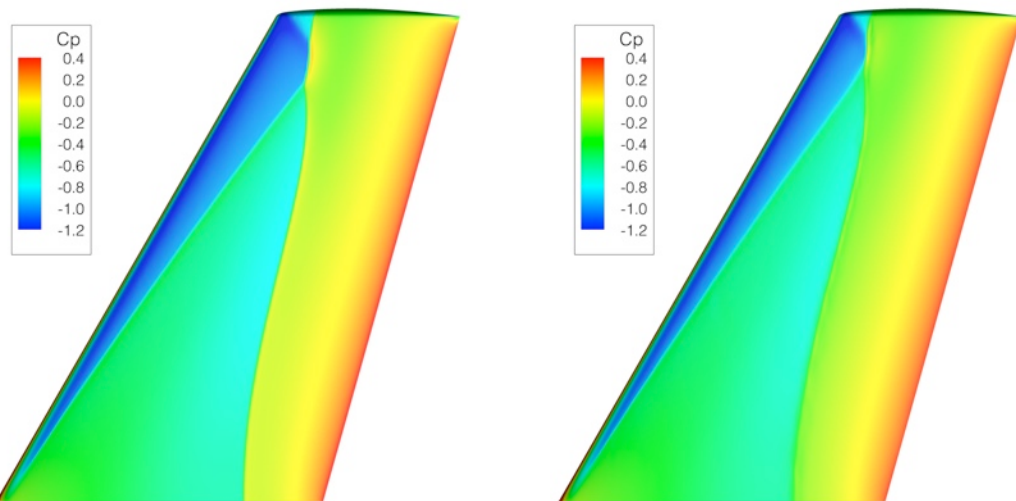

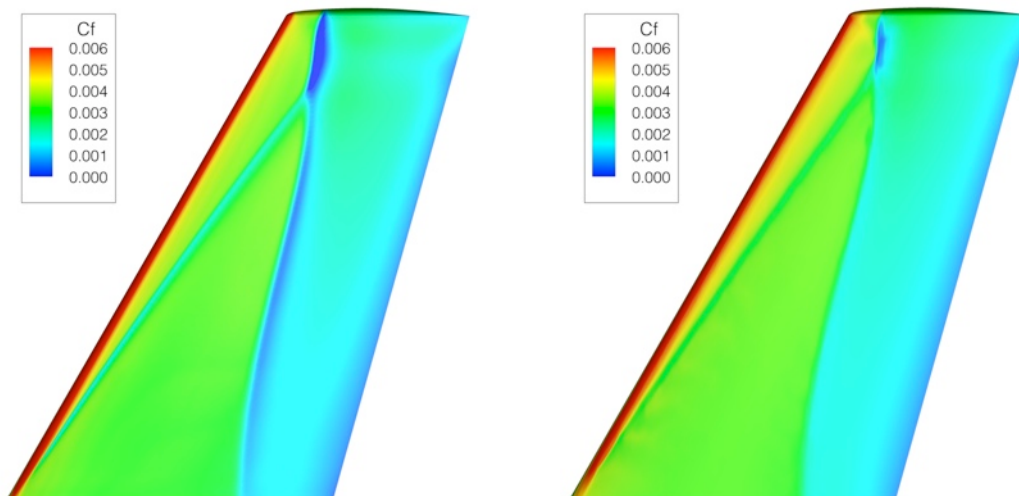**Figure 18. Pressure contours on the Onera M6 wing as computed by Cart3D-Euler (left) and Cart3D-IBL (right).**

Figure 19. Skin friction contours on the Onera M6 wing as computed by CFL3D (left) with the Baldwin-Lomax turbulence model and Cart3D-IBL (right).

DLR-F4 Wing/Fuselage

The first AIAA Drag Prediction Workshop[34] provides another good albeit challenging validation case for the Cart3D-IBL solver. For this case, three separate wind tunnel tests provide not only pressure data but also measured forces at many flight conditions. This case proved to be a challenge for the participants of the workshop itself, at least with the meshes provided. Very few of the Navier-Stokes solvers could match the forces from the experimental data, presumably because they could not properly capture the separation pattern at the trailing edge of the inboard section of the wing. The participants were instructed to compute solutions at fixed lift, which in almost all cases resulted in running solutions at lower angles of attack (up to half a degree lower) than indicated by the wind tunnel data. Note that Aftosmis[12] reported good results with the original Cart3D-IBL solver for this test case.

The improved Cart3D-IBL solver was used generate several solutions on the DLR-F4 at different angles of attack but all at Mach 0.75 and a Reynolds number of 3 million based on the mean aerodynamic chord. The location of the IBL strips are shown in Figure 20; notice both the wing and fuselage were made viscous surfaces. The computed forces from these analyses are shown in Figure 21, along with the result from solutions generated by Buning[35] using the workshop-provided mesh. Cart3D-IBL significantly over-predicts lift, much more so than the Navier-Stokes solutions generated for the workshop. The drag polar is affected accordingly, though the lift-to-drag ratio computed by Cart3D-IBL is much closer to the experimental data. These results clearly indicate a problem in computing lift, even by the Navier-Stokes solver to some extent. In an attempt to improve upon the results of a workshop completed almost a decade ago, the authors took the liberty of generating a new, much finer mesh on the DLR-F4 using the geometry files provided by the workshop online. The results from analysis on this mesh are also shown in Figure 21. The lift prediction has improved though the drag polar is now off slightly. Nevertheless, the reason for the higher lift predicted by Cart3D-IBL is revealed by closer examination of the Navier-Stokes solutions.

Figure 22 shows near-surface-restricted streamlines at the trailing edge of the inboard wing as computed by OVERFLOW on the very fine mesh. Note the extensive, three-dimensional separation pattern at the trailing edge. The workshop results showed a similar separation pattern
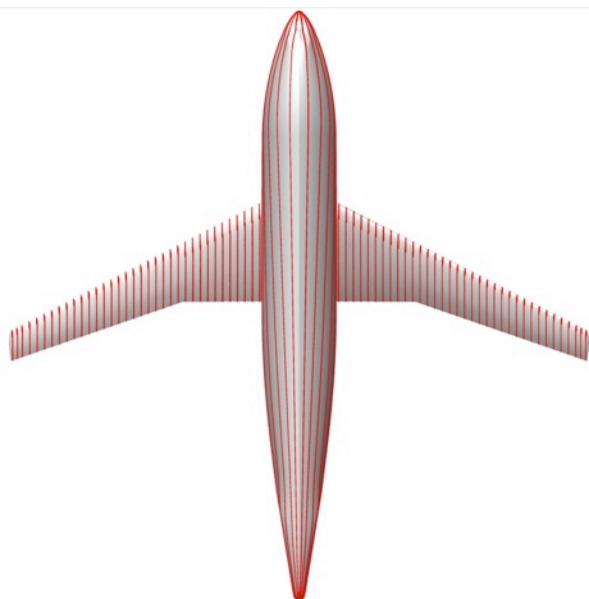

Figure 20. Location of boundary layer strips (red lines) on the DLR-F4 wing-fuselage validation case.
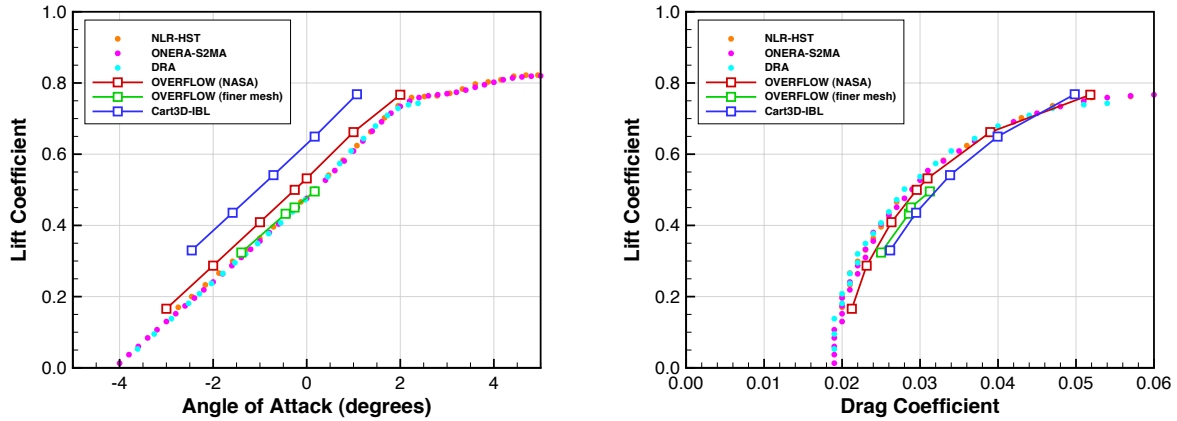
12
American Institute of Aeronautics and Astronautics

Figure 21. Comparison of forces on DLR-F4 wing/fuselage as computed by OVERFLOW and Cart3D-IBL with experimental data.

though not as extensive in the spanwise direction. Also note the severe spanwise turning of the streamlines in trailing edge region. This flow feature seems to be the primary source for the reduction in lift in the Navier-Stokes solution and in the wind tunnel. Cart3D-IBL is not capable of predicting 3-D separation patterns and therefore does not predict any separation. This validation case has simply gone beyond the capability of the current IBL solver.

Nevertheless, the results are still significantly improved from the pure Euler solution. Figure 23 shows pressure distributions computed by Cart3D and Cart3D-IBL compared to experimental data. Note the very significant effects of viscosity as the shock has moved a great deal forward as compared to the inviscid Euler solution, though not quite far enough to match the experimental data. The OVERFLOW solution actually moved the shock too far forward, further indicating that this is a challenging case for even Reynolds-averaged Navier-Stokes solvers.

Recall that Aftosmis also ran this case with the original version of Cart3D-IBL and reported good results for the 40.9% spanwise station as compared to Navier-Stokes results. However, as reported in reference [12], the mesh
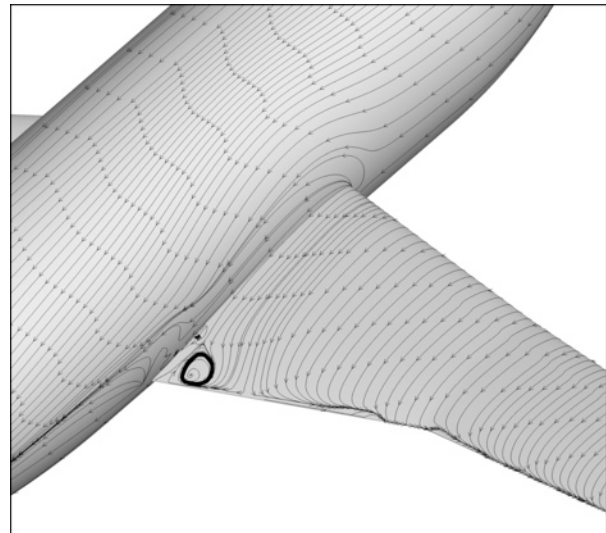

Figure 22. Surface oil-flow pattern at the wing-fuselage junction as computed by OVERFLOW on the DLR-F4. This analysis was generated at $M_\infty = 0.75$, $\alpha = 0.17°$, and $Re_{MAC} = 3.0$ million.

size used was about 2.5 million points for the full-span configuration. The solutions presented here used over 4.3 million points for only half the configuration. Though not presented here, when a smaller mesh that was about the size of that used by Aftosmis was used, the Cart3D-IBL analysis was much more in line with what was presented in reference [12]. In other words, the accuracy of the improved Cart3D-IBL has not been compromised by the improvements presented in this work.

DC-9 Wing/Fuselage/Empennage

To showcase the capabilities of Cart3D-IBL, a more complicated configuration was analyzed. A geometric model of the DC-9 full configuration (without the nacelles and pylons) was generated for this test case. The geometry was analyzed with both Cart3D-IBL and OVERFLOW, though naturally the Cart3D-IBL solution process was much quicker. The geometry is shown in Figure 24 along with the 77 boundary layer strips (mirrored for effect) used in the Cart3D-IBL solution. The OVERFLOW solution was completed on a decent-sized mesh of over 8 million points.

At first, to keep the Navier-Stokes mesh generation simpler, the aircraft was analyzed with no wing/fuselage fairing, very much like the DLR-F4 with hopes of no flow separation. Unfortunately and perhaps predictably, a flow
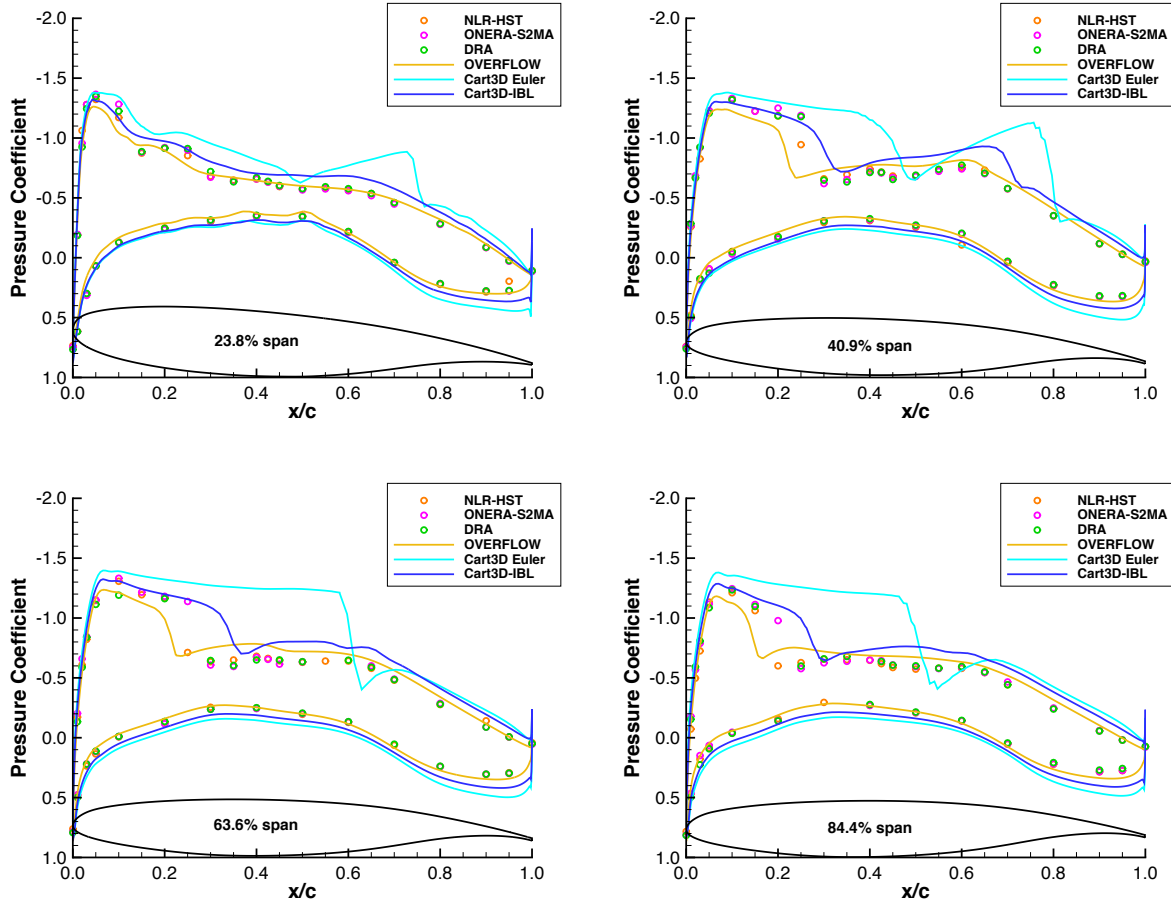
Figure 23. Chordwise pressure distributions at several spanwise stations on the DLR-F4 wing/fuselage at M_∞ = 0.75, Re_{MAC} = 3.0 million, and α = 0.17°. Experimental data, an OVERFLOW solution, and Cart3D solutions are shown (including an Euler solution) for comparison.

separation pattern very much like that shown in Figure 22 was predicted by OVERFLOW. Consequently, a wing/fuselage fairing similar to that on the real aircraft was added to the model which was then reanalyzed. The flow separation was eliminated as shown by the near-surface-restricted streamlines in Figure 25. Also, the streamlines are quite straight and do not turn violently at the trailing edge, indicating healthy, attached flow. On the other hand, the strong shock on the outboard part of the wing does induce separation, but the flow quickly reattaches. The OVERFLOW mesh was quite a bit more complicated and tedious to generate (especially when compared to the Cart3D meshing process), but the result was what was believed to be an excellent validation case for Cart3D-IBL on a complex geometry.

Cart3D Euler and Cart3D-IBL solutions were then generated on this same geometry. The computed pressure distributions at four spanwise stations on the wing are compared to the OVERFLOW solution. The agreement is excellent; the shock location is predicted almost exactly at all stations. For this aircraft, viscous effects effectively move the shock moved upstream just over 5% chord, which is significant. The only major difference in the pressures of the viscous solutions is again at the trailing edge, as we have seen in every validation case presented.

The forces computed by both viscous analyses are given in Table 6, including the drag breakdown. Cart3D-IBL should yield a reasonable prediction for this case, and the forces shown in Table 6 verify this hypothesis. Of course, to be a more proper validation case, a grid refinement study would have to be performed with OVERFLOW to make certain the computed forces are as correct as possible. It is conceivable that a finer mesh will increase the lift and lower the drag of the OVERFLOW solution, bringing the two results even closer. However, considering the first solution generated matched the Cart3D-IBL solution so closely does show promise for the Cart3D-IBL solver. The skin friction distribution as computed by Cart3D-IBL is shown in Figure 27, demonstrating the ability of to model viscosity on all surfaces.
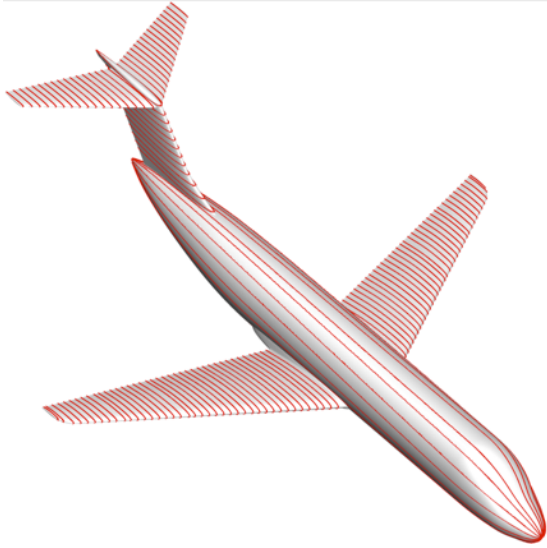
Figure 24. Location of boundary layer strips (red lines) on the DC-9 wing/fuselage/fairing/empennage validation case.
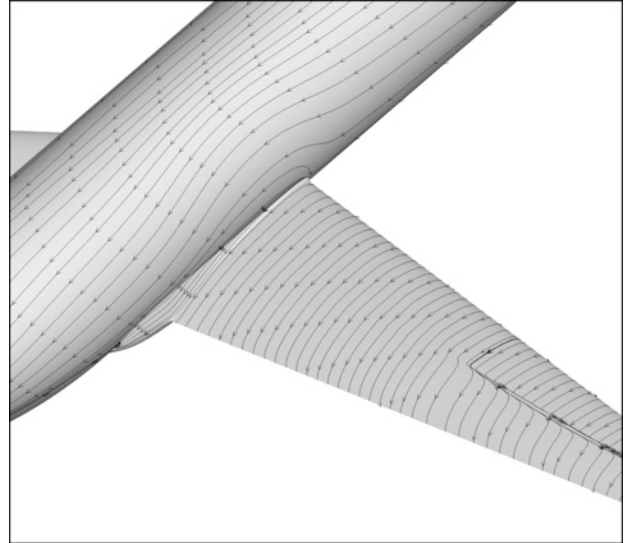

Figure 25. Near-surface-restricted streamlines on the DC-9 wing/fuselage/fairing as computed by OVERFLOW.
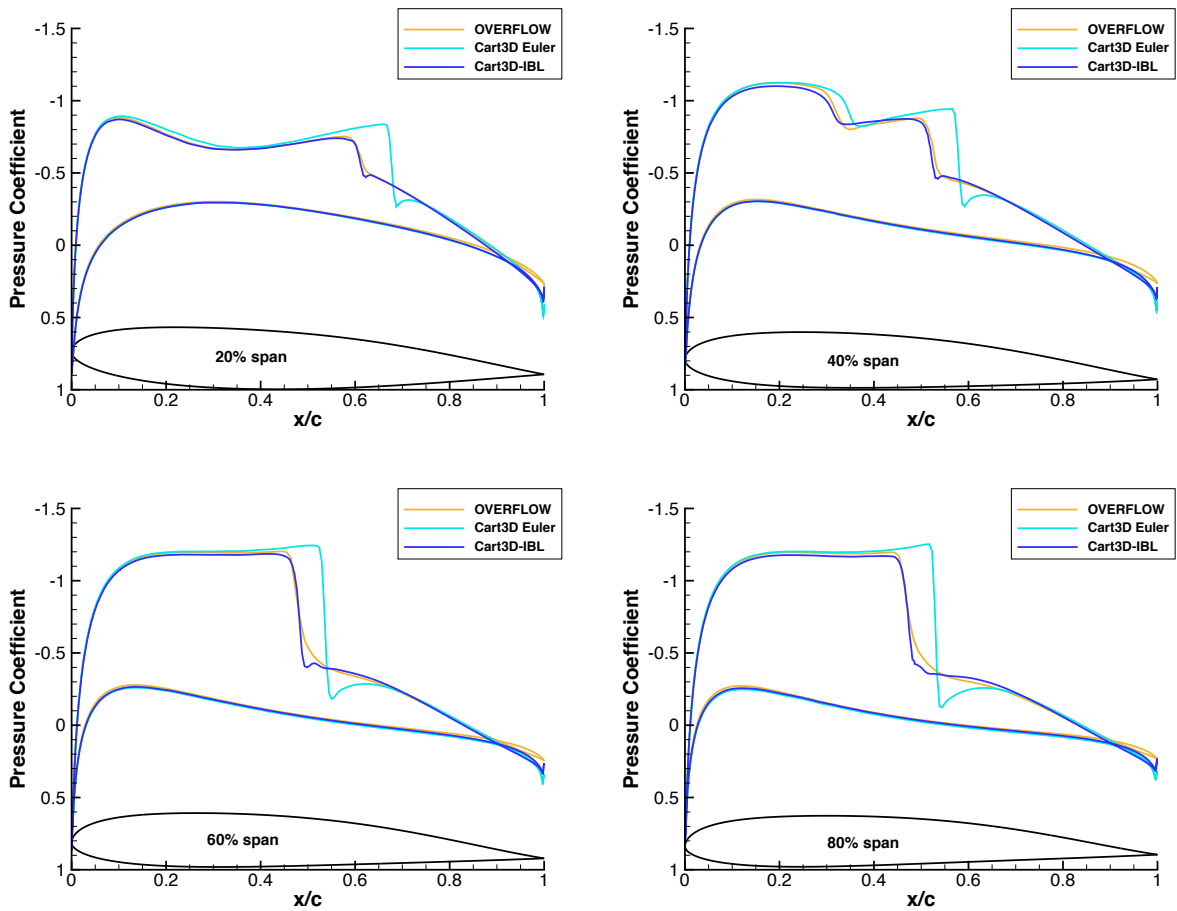

Figure 26. Chordwise pressure distributions at several spanwise stations on the DC-9 wing/fuselage/fairing/empennage model at $M_\infty = 0.78$, $\alpha = 0.5°$, and 31,000 feet of altitude. OVERFLOW and Cart3D-IBL solutions are shown for comparison.

Solver	C_L	C_D	$C_{D,\text{press}}$	$C_{D,\text{visc}}$
OVERFLOW	0.381	0.02506	0.01307	0.01199
Cart3D-IBL	0.386	0.02422	0.01311	0.01110

Table 6. Computed forces on the DC-9 wing/fuselage/ fairing/empennage model analyzed at M_∞ = 0.78, α = 0.5°, and an altitude of 31,000 feet.

IV. Future Work

The work completed on the development of the Cart3D-IBL solver is significant and the developers have made great strides to creating an application ready for production work. But there is certainly a lot more work to do. First and foremost, further validation is necessary. While the number of validation cases presented here is noteworthy, it is not sufficient to provide a final verdict as to the accuracy and applicability of the

Figure 27. Skin friction distribution on the DC-9 model as computed by Cart3D-IBL.

Cart3D-IBL solver. Naturally, the development of the solver to improve accuracy, robustness, and performance will also continue. This section describes just some of the work planned for this solver in the near future.
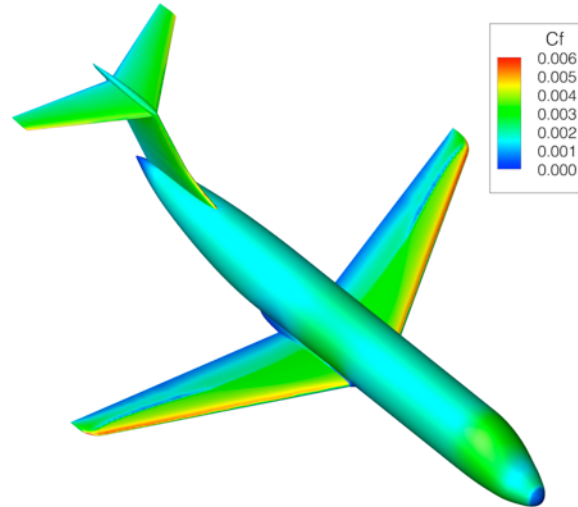
Improvement of Transonic Interaction Law

Every transonic test case on a fine mesh has shown that the IBL interaction law is slightly unstable in the region right after a strong shock. Currently some under-relaxation is used to alleviate this instability. However, this can significantly hinder convergence and is not always sufficient for exceptionally strong shocks. Also, the method can have have difficulty placing the shock. As the shock moves during an IBL update, the boundary layer cannot respond quickly enough, thus inserting a large bump in the displacement thickness where the shock was in the last IBL update. This problem compounds itself when the shock moves to several different locations and the previous boundary layer thickness bumps have not completely disappeared. What would be closer to ideal is a better transonic interaction law, where the approximate inviscid solver can better predict where the shock will be located in the next IBL update. This likely means the inclusion of a transonic flow solver such as a transonic-small-disturbance solver or maybe even a full potential solver. The solver must be exceptionally fast of course, but can exploit the multiple processors that Cart3D uses anyway. Further research in this field will be necessary as the transonic regime is where Cart3D-IBL can have its greatest impact in the industry.

Development of a Wake Model

As mentioned in several parts of the paper, the current implementation of Cart3D-IBL does not have a wake model. It is very difficult to include a 3-D wake model on arbitrary geometry in an unstructured Cartesian mesh. However, the lack of a wake model is clear in the results shown where time after time the trailing edge pressures recover too much and effectively alter the solution in this region. This over-recovery also affects the stability of the boundary layer as it can induce separation in this region where perhaps no separation should occur. The lack of a wake model is a critical issue and should be addressed in the future to ensure accuracy and robustness of the IBL method.

Improving Performance

Currently the only part of the Cart3D-IBL solver that is exploiting multiple processors simultaneously is the original Cart3D Euler solver. None of the IBL parts of the solver are parallelized. They currently do not require a great deal of computation time so it is not a debilitating lack of parallelism. But as the geometry gets more complicated, the meshes correspondingly become larger and the number of boundary layer strips increases. This scenario will become a problem and will hurt the performance of Cart3D-IBL as a design tool. This is especially true for the elliptic solvers (and in particular for the anisotropic solver) which can require the most computational resources during an IBL update. Fortunately there is a great deal of potential for parallelism in the IBL codes. This potential will be tapped in future work as the authors strive to improve the performance of the Cart3D-IBL solver.

Rapid Transition Prediction

The 2-D strip solver in Cart3D-IBL is the default solver, but a second solver has also been partially implemented. A new sweep-taper boundary layer code based of the work of Sturdza[36] has been installed which includes some 3-D effects such as spanwise pressure gradients. This solver exhibits increased accuracy overall but also provides a very unique capability. The sweep-taper solver also includes a rapid transition prediction method, suitable for rapid trade studies and design optimization. The transition prediction method is further detailed in reference [13]. This is a capability not available in Navier-Stokes solvers today and is absolutely critical in the design of modern aircraft that exploit laminar flow. The current sweep-taper solver can only be successfully used in direct mode which does not lend itself to transonic wing analysis. However, development of the quasi-simultaneous version of the solver is underway.

V. Conclusions

The purpose for developing the IBL solver for Cart3D was not to replace or even duplicate Reynolds-averaged Navier Stokes solvers. By definition, IBL methodology can never hope to accomplish that. The purpose for developing Cart3D-IBL was to improve a tool that can do all the things Navier-Stokes solvers *cannot* do presently. The conceptual designer that sketches an airplane for the first time is not going to immediately analyze that sketched geometry with a Navier-Stokes solver. However, Cart3D-IBL can analyze a geometry in about an hour or two on a laptop computer. This is a very powerful tool for the conceptual designer as the design space can be explored more accurately and more thoroughly than with lower fidelity methods. Building massive aerodynamic databases and even using design optimization with high-fidelity aerodynamic analysis suddenly become possible with Cart3D-IBL. While Navier-Stokes based optimization is certainly feasible and has been achieved many times, the massive amount of computer resources currently required to perform the task quickly is not available to most engineers. Also, such optimizations rarely allow the user to make major changes to an aircraft geometry, whereas this is possible and even simple with the Cart3D automatic mesh generation process. Taking this feature into account and based on the results presented above, the Cart3D-IBL solver, even in its fledgling state, has so far proven to be a success. The accuracy of the solver has been demonstrated to be adequate for conceptual and even preliminary design work. The method will inherently have problems computing flows that have complex 3-D separation patterns, but for conceptual design this deficiency is not debilitating. The performance of the solver has not been significantly compromised by adding the IBL solver so it retains that advantage. The robustness of the solver has been significantly improved and should be production-ready shortly. While Navier-Stokes solvers will always be necessary for final validation, the Cart3D-IBL solver allows for improved productivity in the design of aircraft. The additional capabilities, including the ability to predict transition, will allow engineers to design the revolutionary aircraft of the future.

VI. Acknowledgments

References

1. Aftosmis, M. J., Berger, M. J., Melton, J.E., "Robust and efficient Cartesian mesh generation for component-based geometry," *AIAA Journal,* Volume 36, No. 6, pp.952-960, June 1998.

2. Aftosmis, M. J., Berger, M. J., and Adomavicius, G., "A parallel multilevel method for adaptively refined Cartesian grids with embedded boundaries," AIAA 2000-0808, January 2000.

3. Aftosmis M. J., and Berger M. J., "Multilevel error estimation and adaptive h-refinement for Cartesian meshes with embedded boundaries," AIAA 2002-0863, January 2002.

4. Rodriguez, D. L., "Response Surface Based Optimization with a Cartesian CFD Method," AIAA 2003-0465, January 2003.

5. Rodriguez, D. L., "Multidisciplinary Optimization of a Supersonic Inlet Using a Cartesian CFD Method," AIAA 2004-4492, August 2004.

6. Rodriguez, D. L., "Propulsion/Airframe Integration and Optimization on a Supersonic Business Jet," AIAA 2007-1048, January 2007.

7. Sturdza, P., "Extensive Supersonic Natural Laminar Flow on the Aerion Business Jet," AIAA 2007-0685, January 2007.

8. Johnson, F. T., Samant, S. S., Bieterman, M. B., Melvin, R. G., Young, D. P., Bussoletti, J. E., and Hilmes, C. L., "TranAir: A Full-Potential, Solution-Adaptive, Rectangular Grid Code for Predicting Subsonic, Transonic, and Supersonic Flows about Arbitrary Configurations," NASA Contractor Report 4348, pp. 139-141,1992.

9. Chen, L. T. and Bui, M. N., "An Interactive Scheme for Transonic Wing/Body Flows Based on Euler and Inverse Boundary- Layer Equations," AlAA 90-1586, June 1990.

10. Shmilovich, A. and Chang, K. C., "An Algorithm for Predicting the Flow Past Fuselage-Mounted Engine Arrangements," AIAA 92-0151, January 1992.

11. Potsdam, M. A., "An Unstructured Mesh Euler and Interactive Boundary Layer Method for Complex Configurations," AIAA 94-1844, June 1994.

12. Aftosmis, M. J., Berger, M. J., and Alonso, J. J., "Applications of a Cartesian Mesh Boundary-Layer Approach for Complex Configurations," AIAA 2006-0652, January 2006.

13. Rajnarayan, D. and Sturdza, P. , "Extensible Rapid Transition Prediction for Aircraft Conceptual Design," AIAA 2011-3813, June 2011.

14. Sturdza, P., Suzuki, Y., Martins-rivas, H., and Rodriguez, D.L., "A Quasi-Simultaneous Interactive Boundary-Layer Model for a Cartesian Euler Solver," AIAA paper for 50th AIAA Aerospace Sciences Meeting, January 2012.

15. Lock, R.C. and Williams, B.R., "Viscous-Inviscid Interactions in External Aerodynamics," Prog. Aerospace Sci., Vol. 24, pp. 51-171, 1987.

16. Lighthill, M.J., "On displacement thickness," Journal of Fluid Mechanics, Vol. 4, No. 4, pp. 383-392, 1958.

17. Drela, M. and Giles, M. B., "Viscous-Inviscid Analysis of Transonic and Low Reynolds Number Airfoils," AIAA Journal, Vol. 25, No. 10, pp. 1347-1355, Oct. 1987.

18. Drela, M., "XFOIL: An Analysis and Design System of Low Reynolds Number Airfoils," Proceedings of the conference on low Reynolds number aerodynamics, edited by T. J. Mueller, Univ. of Notre Dame, Notre Dame, IN, pp. 1-12, 1989.

19. Green. J. E., Weeks, D. J. and Brooman, J. W. F., "Prediction of Turbulent Boundary Layers and Wakes in Compressible Flow by a Lag-Entrainment Method," Aeronautical Research Council, Reports and Memoranda, No 3791, 1977.

20. Veldman, A. E. P. and Somers, M. A. M., "The Inclusion of Streamline Curvature in a Quasi-Simultaneous Viscous-Inviscid Interaction Method for Transonic Airfoil Flow," preprint, 1998.

21. Carter, J. E., "A New Boundary-Layer Inviscid Iteration Technique for Separated Flow," AIAA 1979-1450, June 1979.

22. Cebeci, T., Chang, K. C., et al., "Viscid/Inviscid Separated Flows," AFWAL-TR-86-3048, ADA179858, 1986.

23. Veldman, A. E. P., "New, Quasi-Simultaneous Method to Calculate Interacting Boundary Layers," AIAA Journal, Vol. 19, No. 1, p. 79, 1981.

24. Saad, Y., *Iterative Methods for Sparse Linear Systems*, PWS Publishing Company, Boston, MA, 1996.

25. Eymard, R., Gallouët, T., and Herbin, R., "Discretization of heterogeneous and anisotropic diffusion problems on general nonconforming meshes SUSHI: a scheme using stabilization and hybrid interfaces," *IMA Journal of Numerical Analysis*, Vol. 30, No. 4, pp. 1009-1043, 2010.

26. Rodriguez, D. L., Sturdza, P., Eymard, R., "Improving the Accuracy of Euler/Boundary-Layer Solvers with Anisotropic Diffusion Methods," AIAA paper for 50th AIAA Aerospace Sciences Meeting, January 2012.

27. Krist, S. L., Biedron, R. T., and Rumsey, C. L., *CFL3D User's Manual*, Version 5.0, NASA TM 1998-208444, NASA, June 1998.

28. Buning, P. G.,Jespersen, D. C., Pulliam, T. H., Klopfer, G. H., Chan, W. M., Slotnick, S. E., Krist, S. E., and Renze, K. J., *OVERFLOW User's Manual*, Version 1.8L, NASA Technical Report, July 1999.

29. Baldwin, B. S. and Lomax, H., "Thin Layer Approximation and Algebraic Model for Separated Turbulent Flows", AIAA 78-257, January 1978.

30. Spalart, P. R. and Allmaras, S. R., "A One-Equation Turbulence Model for Aerodynamic Flows", La Recherche Aerospatiale, Vol. 1, No. 1, pp. 5-21, 1994.

31. Menter, F. R., "Two-Equation Eddy-Viscosity Turbulence Models for Engineering Applications", *AIAA Journal*, vol. 32, no 8. pp. 1598-1605, 1994.

32. Cook, P. H., McDonald, M. A., and Firmin, M. C. P., "Airfoil RAE 2822 -Pressure Distributions, and Boundary Layer and Wake Measurements," in Experimental Data Base for Computer Program Assessment, AGARD-AR-138, pp. A6-1-77, 1979.

33. Schmitt, V. and Charpin, F., "Pressure Distribution on the Onera-M6-Wing at Transonic Mach Numbers," in Experimental Data Base for Computer Program Assessment, AGARD-AR-138, pp. B1-1-44, 1979.

34. Levy, D.W., Zickuhr, T., Vassberg, J., Agrawal, S., Wahls, R.A., Pirzadeh, S., and Hemsch, M.J., "Data Summary from the First AIAA Computational Fluid Dynamics Drag Prediction Workshop," *Journal of Aircraft*, Volume 40, No. 5, pp. 875-882, Sep.-Oct. 2003.

35. Lee-Rausch, E. M., Buning, P. G., Morrison, J. H., Park, M. A., Rivers, S. M., Rumsey, C. L., and Mavriplis, D., "CFD Sensitivity Analysis of a Drag Prediction Workshop Wing/Body Transport Configuration," AIAA 2003-3400, June 2003.

36. Sturdza, P., *An Aerodynamic Design Method for Supersonic Natural Laminar Flow Aircraft*, Ph.D. Dissertation, Stanford University, Dec. 2003.